An Inverse CFD Actuator Disk Method for Aerodynamic Design and Performance Optimization of Horizontal Axis Wind Turbine Blades

M. N. Hamlaoui[a,c,*], A. Bouhelal[a], A. Smaili[a], S. Khelladi[b] and H. Fellouah[d]

[a]*Laboratory of Green and Mechanical Development (LGMD), National Polytechnic School -ENP-, P.B. 182 El-Harrach, Algiers, 16200, Algeria*
[b]*Laboratoire d'Ingénierie des Fluides et des Systèmes Énergétiques (LIFSE), 151 boulevard de l'Hôpital, 75013, Paris, France*
[c]*Department of Civil Engineering, Université de Ferhat Abbas Setif 1, Route de Béjaia, Setif, 19000, Algeria*
[d]*Department of Mechanical Engineering, Université de Sherbrooke, 2500 Boulevard de l'Université, Sherbrooke (QC) J1K2R1, Canada*

ARTICLE INFO

Keywords:
Horizontal Axis Wind Turbines
Inverse actuator disk method
Aerodynamic design
Blade linearization
Annual energy production
Near wake

ABSTRACT

In this study, advanced design technique has been introduced to determine the radial local chord distribution on the rotor blades of Horizontal Axis Wind Turbines (HAWTs) based on an inverse CFD actuator disk method combined with linearization of both the chord and twist distributions. The overarching goal was to refine HAWT rotor blade design for enhanced aerodynamic performance. The proposed design methodology, embedded into a custom axisymmetric Computational Fluid Dynamics (CFD) subroutine based on the actuator disk model in OpenFOAM, incorporates key aerodynamic factors such as turbulence, viscosity, and both two-dimensional and three-dimensional flow field properties. Results from this innovative approach indicate that rotor models crafted using our algorithm significantly outperform those based on traditional theories in terms of efficiency and consistency. Comprehensive aerodynamic analyses focusing on the power coefficient and annual energy production (AEP) across various incoming free stream velocities show that the optimized model improves power coefficient by up to 70% and AEP by 17.64% compared to the baseline model. Additionally, the optimized model demonstrates a 15% reduction in velocity deficit, enhancing the potential for optimizing wind farm layouts.

Nomenclature

Abreviations

ADM	Actuator Disk Method
AEP	Annual Energy Production
AMWS	Annual Mean Wind Speed
BEM	Blade Element Momentum
CFD	Computational Fluid Dynamics
HAWT	Horizontal Axis Wind Turbines
HPC	High Performance Computing
MEXICO	Model EXperiments In Controlled cOnditions
NREL	National Renewable Energy Laboratory
SIMPLE	Semi-Implicit Method for Pressure-Linked Equation

*Corresponding author
mohammed_nadjib.hamlaoui@g.enp.edu.dz (M.N. Hamlaoui)
ORCID(s): 0000-0002-5269-074X (M.N. Hamlaoui)

Symbols

α	Angle of attack (deg)
α_{op}	Optimum angle of attack (deg)
α_s	3D stall angle of attack (deg)
β	Twist angle (deg)
η	Rotor efficiency (%)
γ	Coning angle (deg)
λ	Tip Speed Ratio
λ_r	Local Tip Speed Ratio
Ω	Speed of rotation (rad/s)
ϕ	Flow angle (deg)
σ	The rotor local solidity
θ_0	Pitch angle (deg)
ξ	Blade chord and twist linearization root
a, a'	Axial and Tangential induction factors
c	Local chord at given radial station (m)
c'	Weibull scale parameter (m/s)
C_l, C_d	The corrected lift and drag coefficients
C_n, C_t	Normal and Tangential force coefficients
C_p	Rotor power coefficient
C_T	Rotor thrust coefficient
dP	Elementary power output (W)
dQ	Elementary mechanical torque (N.m)
f_θ	Tangential volume force component (N/m^3)
f_s, f_d	Shift parameter and Separation factors for the lift and for the drag coefficients variation
f_z	Axial volume force component (N/m^3)
k'	Weibull shape parameter
P	Power output (W)
P_{wind}	Kinetic energy of the wind (W)
Q	Mechanical torque (N.m)
R	Rotor radius (m)
r	Local radial station (m)

T	Thrust force (N)
U_0	Free stream velocity (m/s)
U_{Design}	Design wind speed (m/s)
U_n	Normal component of the flow velocity relative to blade local station (m/s)
U_{rel}	Flow velocity relative to the blade radial station (m/s)
U_t	Tangential component of the flow velocity relative to blade local station (m/s)

1. Introduction

In the last decades, renewable energy has become a pertinent alternative energy source of the fossil fuels due to their harmful environmental impact and huge carbon dioxide gas emissions causing the mostly well-known green house effect [1]. Wind energy as sustainable, clean and renewable energy source has been considered as one of the most efficient alternatives where it has known a large amount development in the previous years [2]. Mainly, wind turbines converts the kinetic energy of the wind to an electrical power used to supply human needs. As the wind turbine blades represents the key element for the wind kinetic energy absorption, it should be effectively designed to capture as much power as possible yielding high mechanical system efficiency as well as decreasing the energy cost [3]. The main purposes of the aerodynamic design and optimization of wind turbines is to find the best way among several candidate's approaches, based on computer codes, providing the highest accuracy as well as easiest and fastest predictions [4]. Basically, the annual energy capacity [5], the maximum power output [6] and the energy cost [7] are considered as the most selected objective functions used during the Horizontal Axis Wind Turbine (HAWT) design and optimization process.

Accurate predictions of loads remain crucial during the design process of HAWT rotor blades; a certain over/under estimation of the aerodynamic performances leads to system being over/under designed which affects mainly the energy costs. Primarily, three formulations are presented in the literature to fulfill the aerodynamic analysis around HAWT rotor which are classified as follows: (i) Integral methods (Blade Element Momentum (BEM) method [8, 9, 10], Vortex lattice method [11], Vortex/Source panel methods [12], etc), (ii) Hybrid methods (including: Actuator disk method [13, 14, 15], Actuator line method [16, 17], and Actuator surface method [18, 19]) and (iii) Full Navier-Stokes method [20, 21, 22, 23, 24]. The Full Navier-Stokes method turns out to be the most accurate method for HAWT performance predictions as well as the wake study around the rotor [20, 10]. However, it remains expensive due to the long calculation time and high performance computing requirements which continues to display irregularities for industrial purposes [22].

The concept of the actuator disk, particularly in its analytical iterations such as the Blade Element Momentum (BEM) method, has become the predominant model for predicting the performance and facilitating the design and optimization of rotor blades for HAWT [9, 25, 26]. Originally introduced by Rankine [27] and Froude [28] for propeller applications, the model was initially conceptualized as a stationary disk. Subsequent enhancements by Joukowski [29] incorporated the dynamics of a rotating disk, and Betz [30] later quantified the maximum power extraction achievable by an ideal rotor. Further refinements by Glauert [31] integrated two-dimensional flow effects and the impact of blade loads on the HAWT rotor, leading to the formalization of the BEM method. This method merges blade element theory, which computes lift and drag forces along the blade span, with momentum theory, assessing the momentum balance within the annular stream tube as it passes through the rotor [32].

Widely adopted by both industrial and academic entities, the BEM method serves as a cornerstone for the design, optimization, and performance analysis of HAWTs [9, 25, 33, 8]. Techniques such as the inverse BEM [34, 35] and the inverse actuator disk method [36, 37] enable the determination of non-linear chord and twist distributions along the turbine blade at the initial design stages [32]. Linearization of these distributions is critical for simplifying construction and reducing material costs. Several strategies for linearizing the blade chord have been proposed. For instance, Tahani et al. [38] evaluated multiple airfoil families to design a 1 MW HAWT and identified the optimal blade span positions for maximizing power output, suggesting that the most effective region for chord linearization lies between 53% and 67% of the blade span. Additionally, Yang [33] conducted an extensive investigation on the NREL-5MW baseline wind turbine using the NREL-FAST code, aiming to enhance its aerodynamic performance through chord linearization techniques. The results indicated significant improvements in performance, particularly at

lower wind speeds. More recently, Alkhabbaz et al. [39] undertook an aerodynamic study for a 10 kW HAWT design based on ideal distributions of chord and twist, subsequently applied to a realistic rotor model, and determined that the radial station at $r/R = 0.3$ offers an optimal root for linearization processes. This design approach aligns with the safety standards stipulated by the International Electrotechnical Commission (IEC) in IEC 61400-2, which outlines guidelines for small wind turbines, defined as those with a rotor swept area less than 200 square meters and a rated output around 50 kW [40].

Despite analytical methods use fast processing one-dimensional (1D) codes providing pretty good results, however, they posses specific critical aspects [41]. In contrary to the Full Navier-Stokes method, the BEM method is known as low order rotor model which relies on the flow independence principle neglecting the interaction between contiguous span wise positions flow effects. The mentioned independency causes the resulting thrust and torque to be over-estimated [42]. Corrections are primordial to account the pressure equalization along the rotor blade causing the sectional axial and tangential forces being over-predicted. Mainly, two different techniques have been embraced as an approach to correct low order type methods [41, 43, 44]:

- The first concept consists on correcting the resulting rotor blade loads prior to their application to the flow field.
- The second approach corrects the 2D lift and drag coefficients to adopt 3D behavior which rely on the lift coefficient increment and the drag coefficient decrement.

In addition to the limitations mentioned above, the BEM method requires additional corrections for the momentum, the turbulence, viscosity and the 2D/3D flow field considerations [31, 45].

The literature shows clearly the limitation of the most used BEM method to design HAWT which excludes the effects of turbulence, viscosity, pressure non-uniformity and the 2D/3D flow field considerations. In this paper, an analytical local chord distribution over the rotor blade, local chord and twist linearization technique have been proposed. For this purpose, the HAWT rotor has been described by a CFD axisymmetric Actuator Disk Method (ADM) and the flow-field has been modeled by the RANS equations coupled to the mostly well-known two equations $k - \omega$ SST turbulence model [46]. The mathematical model developed has been integrated into a subroutine in OpenFOAM. The accuracy of this numerical method was validated using the MEXICO rotor [47, 48]. Additionally, the effectiveness of the design algorithm was demonstrated by optimizing the aerodynamics of both the MEXICO and the NREL Phase VI small HAWT [49, 50].

2. Mathematical Model

2.1. Actuator Disk Model

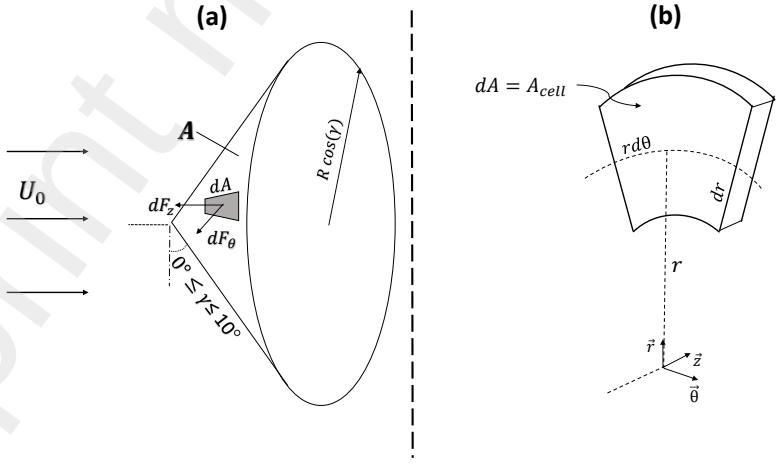

Figure 1: Actuator disk concept.

The Actuator Disk Concept encapsulates the simplified mathematical representation of a real horizontal axis wind turbine (HAWT) structure. It conceptualizes the rotor as a circular cone, delineated by the rotor's swept area A. The cone's base, with a diameter of $R\cos(\gamma)$, models the physical impact of the rotor on the flow field. In this model, γ represents the coning angle, typically varying from 0° to 10°, and R is the length of the rotor blade. The rotor's external forces, calculated for each mesh cell within the actuator disk volume, oppose the incoming airflow and induce a pressure differential. Notably, this generalized model stipulates that the rotor-induced forces impart no radial force ($dF_r = 0$), resulting in forces being broken down into axial (dF_z) and tangential (dF_θ) components as illustrated in Fig. 1.(a).

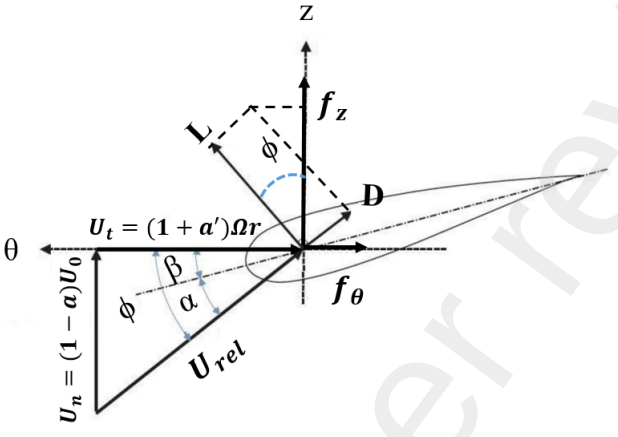

Figure 2: Sectional forces and velocity vectors relative to the blade radial station r.

The Blade Element Theory offers a prevalent framework for estimating sectional forces along the rotor blades of a HAWT. Typical rotors are comprised of B blades, each extending a length R, with speed of rotation Ω and a predefined pitch angle θ_0. The blade's chord c and twist β are configured to ensure radial variation from the root to the tip. Sectional loads, generated by the rotor and acting at a specific radial position r, derive from the aerodynamic lift and drag as shown in Fig. 2. Here, the relative flow velocity U_{rel} at the blade's radial station decomposes into normal U_n and tangential U_t components:

$$U_{rel} = \sqrt{U_n^2 + U_t^2} \tag{1}$$

$$\text{where} \quad U_n = -u_j z_j \quad \text{and} \quad U_t = (\Omega r - u_j \theta_j) \tag{2}$$

Here, u_j denotes the local velocity component, with z_j and θ_j representing the cosine directors of the unit vectors z and θ.

The geometric angle of attack α is defined as:

$$\alpha = \arctan(\frac{U_n}{U_t}) - (\beta + \theta_0) \tag{3}$$

To integrate the actuator disk's assumption of an infinite number of blades, adaptations like the tip loss correction factor proposed by Shen et al. [45] have been incorporated, enhancing the Navier-Stokes based actuator approaches:

$$F = \frac{2}{\pi}\cos^{-1}[\exp(-g\frac{B(1-\frac{r}{R})}{2\frac{r}{R}\sin\phi})] \tag{4}$$

$$g = \exp(-a(B\lambda - b)) + 0.1 \tag{5}$$

where a and b are constants of 0.125 and 21 respectively.

Based on Blade Element Theory, the resultant blade sectional loads in the axial f_z and tangential f_θ directions at a given radial station r are expressed as:

$$f_z = \frac{1}{2}\rho U_{rel}^2 c F C_n \qquad \text{where} \quad C_n = (C_l \cos\phi + C_d \sin\phi) \tag{6}$$

$$f_\theta = \frac{1}{2}\rho U_{rel}^2 c F C_t \qquad \text{where} \quad C_t = (C_l \sin\phi - C_d \cos\phi) \tag{7}$$

The actuator disk subroutine operates using the O-type structured hexahedral mesh cells as shown in Fig. 1.(b). The resultant external loads applied by the HAWT rotor, computed at discrete points defining the mesh cell center located inside the predefined cylindrical actuator disk volume, are expressed as follows:

$$dF_i = F_{cell,i} = B f_i dr \frac{r d\theta}{2\pi r} = \frac{B}{2\pi} f_i \frac{A_{cell}}{r} \tag{8}$$

The source term S_i, representing the external forces, should be introduced in the momentum equation as a volume force, resulting in the following expression:

$$S_i = \frac{F_{cell,i}}{V_{cell}} \tag{9}$$

Once the sectional forces are estimated, the aerodynamic performances of the simulated HAWT can be evaluated as follows:

$$\begin{cases} dQ = dF_\theta \times r \\ dP = dQ \times \Omega \\ P_{wind} = \frac{1}{2}\rho A U_0^3 \\ T = B\sum_1^n dF_z \\ P = \sum_1^n dP \\ C_p = \frac{P}{P_{wind}} \end{cases} \tag{10}$$

where dQ, dP, P_{wind}, T, P and C_p denote, respectively, the elementary torque, the elementary mechanical power, the wind kinetic energy, the rotor thrust force, the total mechanical power and the rotor power coefficient.

2.2. 3D flow correction model

The fundamental operation of the actuator disk model assumes a quasi two-dimensional flow, neglecting the interactions at various radial sections. However, practical scenarios typically involve spanwise flows, which are not accounted for by the simplistic blade element method [44]. Therefore, it becomes imperative to apply three-dimensional corrections to better represent the effects of blade rotation. This study incorporates a correction model from the recent work of Hamlaoui et al. [51], described briefly below in the context of HAWT performance:

$$\begin{cases} C_l &= (1 + f_s) C_{l,2d} \\ C_d &= (1 + f_d) C_{d,2d} \end{cases} \tag{11}$$

The correction to the lift coefficient utilizes a Gaussian function, as shown in Eq. (11), where the parameters a, α_s, and d signify the amplitude, the angle of attack at maximum lift (or 3D stall angle), and the width of the peak, respectively. These parameters are set as follows: $a = 1.55$, $\alpha_s = 24.96\left(\frac{r}{R}\right)^{-0.117}$, and $d = 9.5$.

$$f_s(\alpha, \frac{r}{R}) \quad = a(1 - (\tfrac{r}{R})^2) \exp(-(\tfrac{\alpha - \alpha_s}{d})^2) \tag{12}$$

Regarding the drag coefficient, they suggested modifications to the widely recognized Chaviaropoulos and Hansen drag correction model [52], which initially overestimates certain aspects, to refine its predictions. The modified expression is:

$$f_d = a_h(\tfrac{c}{r})^h \cos^n(\beta) \tag{13}$$

where a_h is adjusted to 1.2 from the original 2.2, with $h = 1$ and $n = 4$.

3. Governing Equations

The flow field around the HAWT rotor is analyzed using the Reynolds Averaged Navier-Stokes (RANS) approach, where the resulting time-averaged equations are presented as follows:

$$\frac{\partial u_i}{\partial x_i} = 0 \tag{14}$$

$$u_j \frac{\partial u_i}{\partial x_j} = -\frac{1}{\rho}\frac{\partial p}{\partial x_i} + \frac{\partial}{\partial x_j}[(\nu + \nu_t)\frac{\partial u_i}{\partial x_j}] + S_i \tag{15}$$

Here, u_i represents the fluid absolute velocity, p is the pressure, and ν and ν_t denote the kinematic laminar and turbulent viscosity, respectively. S_i is the source term representing the actuator disk body force acting upon the flow field. For the closure of the RANS algebraic system of equations, the two-equation k-ω Shear Stress Transport (SST) turbulence model is utilized, known for its efficiency in prediction and less sensitivity to free stream conditions [53].

4. HAWT Design

In the present section, the local chord distribution, the local chord and twist linearization techniques and the new design process algorithm, applied for HAWT design, will be developed and presented.

4.1. Local chord distribution

Fig. 2 depicts the sectional forces and velocity vectors relative to the blade radial station obtained based on the blade element theory. The equations used to calculate both the elementary axial and tangential force components are presented as follows:

$$\begin{cases} dF_n = \frac{1}{2}B\rho U_{rel}^2 cFC_n dr \\ dF_t = \frac{1}{2}B\rho U_{rel}^2 cFC_t dr \end{cases} \tag{16}$$

On the other side, the elementary axial and tangential force components can be determined based on the conservation of momentum principle yielding the following equations [54]:

$$\begin{cases} dF_n = 4a(1-a)\rho U_0^2 F\pi r dr \\ dF_t = 4a'(1-a)\rho U_0 \Omega F\pi r^2 dr \end{cases} \tag{17}$$

The analytical formulations found in the literature, applied to extract the local chord distribution along the blade span direction, are mainly based on the axial force component because of the challenging and unpredictable conditions caused by wind shear and trailing vortices, which greatly affect the sensitivity of the tangential force component [55]. Nevertheless, from a technical point of view, the optimum design shape for a given rotor diameter is a HAWT which captures as much power as possible. Manwell [54] has demonstrated that an optimal blade shape should account for the impact of wake rotation while disregarding drag coefficient ($C_d = 0$) and tip losses ($F = 1$). Thus, the impact of axial and tangential force components would be included in the development of the new analytical model for local chord estimation along the blade radial stations.

The division of the elementary tangential force component to the axial force component yields the following expression:

$$\frac{a'}{a} = \frac{1}{\lambda_r}\frac{C_t}{C_n} \approx \frac{1}{\lambda_r} tan(\phi) \qquad \text{where : } \lambda_r \text{ is the local tip speed ratio} \tag{18}$$

By equalizing both Eq. (16) and Eq. (17) for the elementary tangential force component than multiplying and dividing it by Ω and dividing both sides by the global radius R, a more concise expression for the local chord distribution is obtained, presented as follows:

$$\frac{c(r)}{R} = \frac{2\pi C_T}{BC_l sin(\phi)} \frac{U_0^2}{U_{rel}^2} \frac{\lambda_r}{\lambda} tan(\phi) \tag{19}$$

where $\lambda = \frac{\Omega R}{U_0}$ is the global tip speed ratio.

The main objective, to develop a consistent chord distribution, consists on optimizing the output mechanical power as well as the rotor efficiency (η) of the HAWT rotor. Thus, the thrust coefficient would be replaced based on the efficiency formulation expressed as follows:

$$\eta = \frac{P}{TU_0} = \frac{C_p}{C_T} \tag{20}$$

During the HAWT design process using a given airfoil profile at a predefined Reynolds number, the optimum design point is chosen as the angle of attack (α_{op}) providing the highest glide ratio ($\frac{C_{l,op}}{C_{d,op}}$) which must be conserved along the rotor blade. At this design point, the HAWT rotor is expected to operate at the optimal conditions where the axial induction factor $a \to \frac{1}{3}$ providing a maximum power generation (C_p=$C_{p,max}$=$\frac{16}{27}$), maximum efficiency (η= $\frac{2}{3}$).

Consequently, the yielding optimal chord distribution formulation is expressed as follows:

$$\frac{c(r)}{R} = \frac{16\pi}{9BC_{n,op}} \frac{U_0^2}{U_{rel}^2} \frac{\lambda_r}{\lambda} \tag{21}$$

4.2. Blade chord and twist linearization

From a technical perspective, it is essential to linearize the chord and twist distributions to streamline the manufacturing process and minimize material costs [39]. In our study the blade tip would be considered as fixed root for the linearization process while any radial station along the blade span could be considered as root in order to determine the floating amount of first profiled span wise position providing the best rotor performances. Thus, the linear chord and twist distribution can be estimated as follows:

$$\begin{cases} c(r_i) = c_{root} + [\frac{c_{tip} - c_{root}}{(\frac{r}{R})_{tip} - (\frac{r}{R})_{root}}]((\frac{r}{R})_i - (\frac{r}{R})_{root}) \\ \beta(r_i) = \beta_{root} + [\frac{\beta_{tip} - \beta_{root}}{(\frac{r}{R})_{tip} - (\frac{r}{R})_{root}}]((\frac{r}{R})_i - (\frac{r}{R})_{root}) \end{cases} \tag{22}$$

4.3. Design process algorithm

The actuator disk concept represents an idealized rotor through a mathematical model grounded on four primary assumptions: (a) the flow of fluid through the control volume is idealized as inviscid, incompressible, and irrotational without the influence of turbulence, (b) it presumes an infinitely large number of blades, (c) it assumes that the flow is uniform and one-dimensional across the surface of the disk, and (d) it considers that the static pressure remains unchanged both far upstream and downstream of the rotor. Even though, different corrections have been proposed to take into account some limitations [29, 30, 31, 45], the analytical approach is still inconsistent and breakdown for several cases. To account of the turbulence, viscous, the non-uniformity and the 2D/3D flow field considerations, a hybridisation of the BEM/Navier-Stokes equations, during the design process of the blade, has been carried out in the present work. The whole design algorithm, governing the chord and twist computations, has been summarized in two main parts.

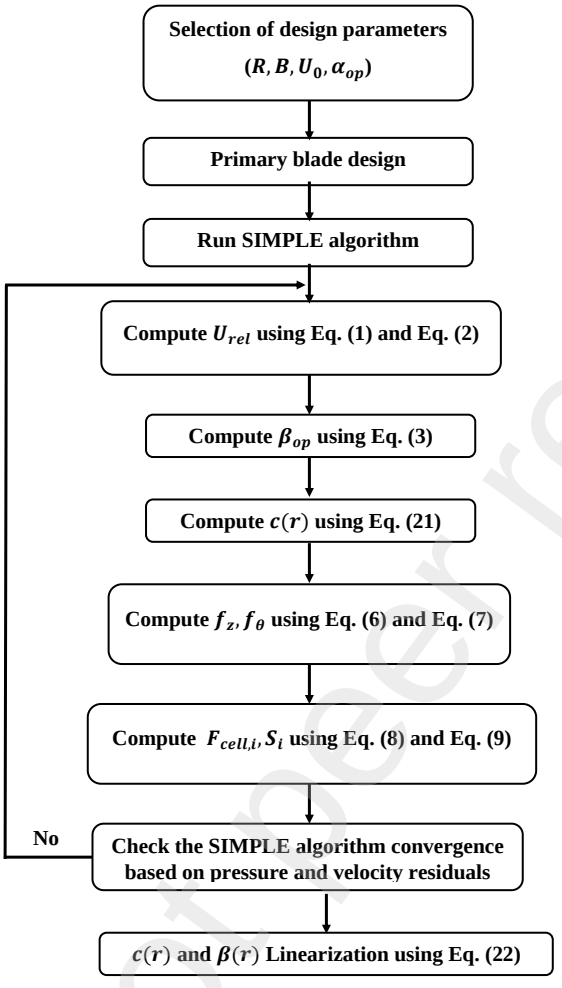

Figure 3: Flow chart of the primary blade design, local chord and twist linearization algorithm.

The primary blade design, chord and twist linearization algorithm providing both the non-linear and the linear chord and twist distributions, as depicted in Fig. 3, has been highlighted as follows:

1. Select the design parameters (R,B,U_0,α_{op}).
2. Run the Semi-Implicit Method for Pressure-Linked Equation (SIMPLE) algorithm.
3. Compute the flow velocity relative to the blade radial station (U_{rel}) using Eq. (1) and Eq. (2).
4. Compute the optimal twist angle of the primary design using Eq. (3).
5. Compute the local chord using Eq. (21).
6. Compute the sectional forces f_z and f_θ using Eq. (6) and Eq. (7) respectively.
7. Compute the surficial forces $F_{cell,i}$ and the source term S_i using Eq. (8) and Eq. (9).
8. Check the SIMPLE algorithm convergence based on pressure and velocity residuals, repeat from Step (3) or else finish.
9. Process the chord and twist linearization using Eq. (22).

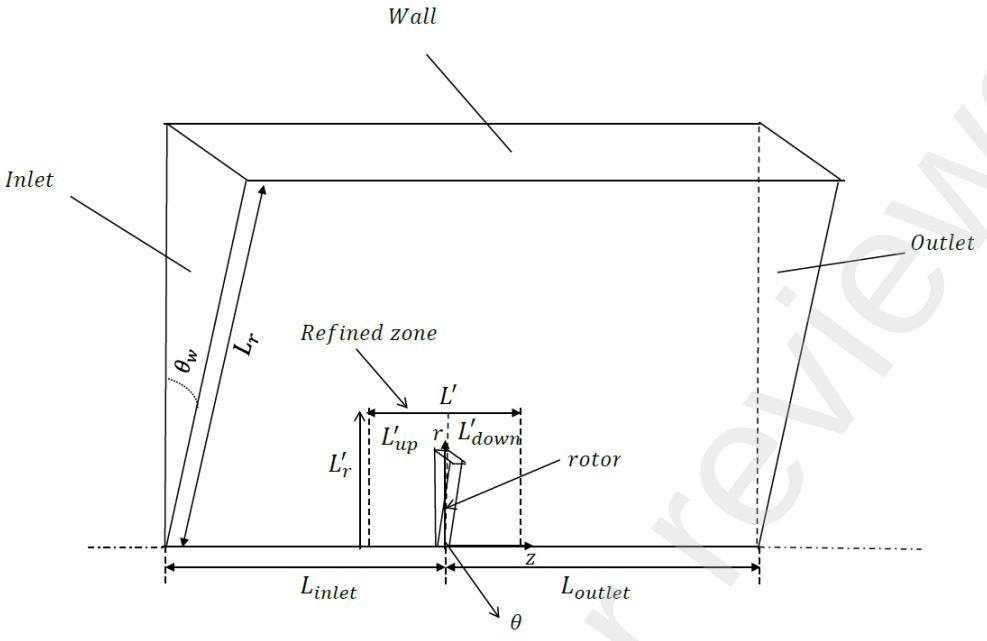

Figure 4: Actuator disk computational domain illustration.

5. Numerical Method

The design and performance assessment of the actuator disk involved calculations performed with a custom OpenFOAM subroutine previously developed by Hamlaoui et al. [56, 13]. This subroutine utilizes the Finite Volume method for discretizing the Navier-Stokes equations in cylindrical coordinates.

For simulations of axisymmetric flows, the computational domain is set up as a wedge geometry with a small angle ($\theta_w \leq 5^o$), in accordance with guidelines from the OpenFOAM user manual [57] (refer to Fig. 4). This geometry is defined by a radial distance of L_r= 5D and an axial length of 10D. The domain along the axial direction is structured around the rotor center, segmented as follows:

- The inlet boundary condition is positioned 4.5D upstream from the rotor's central point.
- The outlet is placed 5.5D downstream from the rotor center.
- Near the rotor, the domain features a finely meshed area extending 1D in both the upstream and downstream directions, with a radial extent of L'_r= 1D.

The computational mesh throughout the domain employs an O-type structured hexahedral mesh, as illustrated in Fig.5, organized into 20 mesh blocks. The regions with significant flow gradient variations are finely meshed, while the remaining areas are discretized with a mesh of adequate size to guarantee the convergence of numerical solutions. According to the mesh sensitivity analysis discussed in Sec.A, the optimal configuration for actuator elements along the rotor blade span was found to be N_b= 128, with an optimal mesh size of D/128 for both the upstream and downstream refined areas. The total mesh comprised approximately 6.7x10^3 cells, which was implemented during the Horizontal Axis Wind Turbine (HAWT) design phase.

The computational setup for the actuator disk method incorporates specific boundary conditions, outlined as follows:

- **Inlet Boundary Condition:** The domain's inlet is defined by a uniform profile for velocity, turbulence kinetic energy, and specific dissipation rate as $U = (0, U_0, 0)$, $k = (0, k_0, 0)$, and $\omega = (0, \omega_0, 0)$ respectively, where U_0 is the free stream velocity. The turbulence parameters k_0 and ω_0 (initial values for turbulent kinetic energy and specific dissipation) are based on the OpenFOAM user guide [57], as demonstrated in Eq. (23). Here, I, C_μ, L,

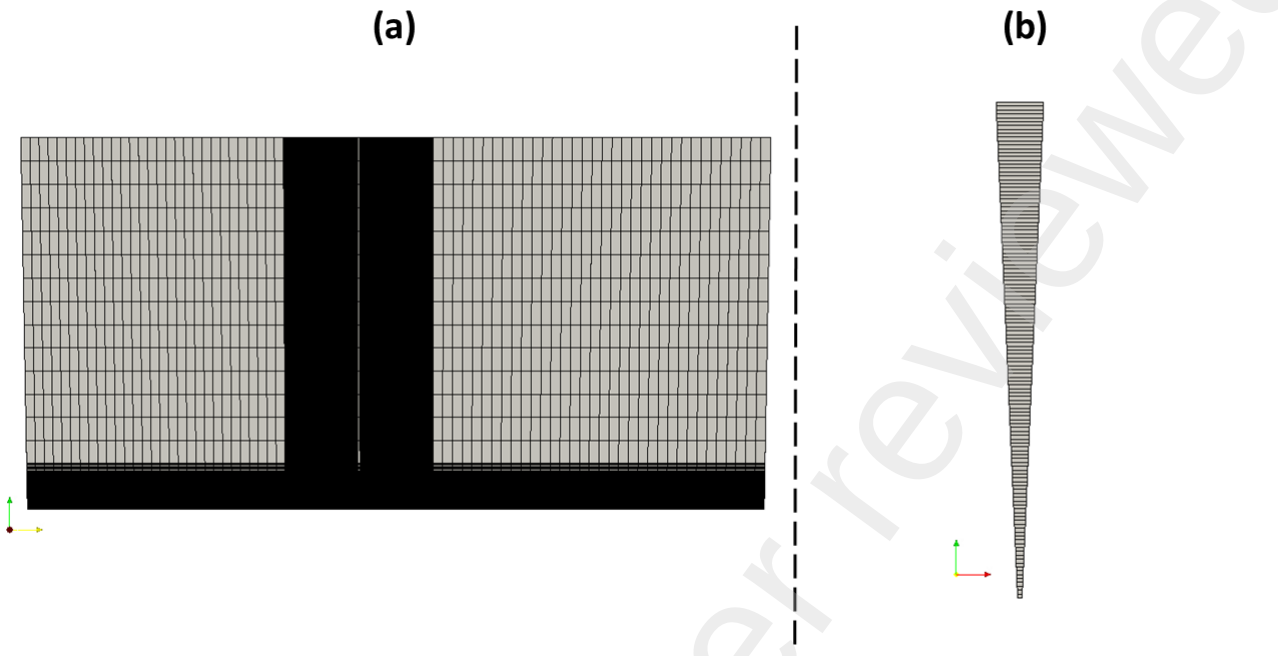

Figure 5: O-type structured hexahedral mesh discritization over (a) the computational domain and (b) the wind turbine rotor.

and I represent the turbulence intensity, a constant value of 0.09, a reference length scale, and the characteristic flow length, approximately 0.7 times the HAWT blade radius, respectively.

- **Outlet Boundary Condition:** A zero gradient condition is prescribed for velocity, turbulence kinetic energy, and specific dissipation rate at the outlet, with a pressure outflow specified for the pressure field.
- **Wall Boundary Condition:** A slip condition is applied to the lateral wall boundaries to prevent shear stress effects on the flow.

This arrangement ensures the computational model closely simulates the physical conditions anticipated in real-world scenarios involving an actuator disk.

$$\begin{cases} k_0 = \frac{3}{2}(U_0 I)^2 \\ \omega_0 = \frac{k_0^{0.5}}{C_\mu^{0.25} L} \\ L = 0.07l \end{cases} \tag{23}$$

For the computational fluid dynamics (CFD) simulations, we employed a second-order difference scheme to discretize the spatial components of the Navier-Stokes equations, while the convective terms were handled using a second-order Gauss Upwind scheme. To address the axisymmetric Navier-Stokes equations for steady-state incompressible turbulent flows, the SIMPLE algorithm was utilized. Additionally, relaxation factors were implemented, with values set at 0.3 for pressure and 0.7 for other variables.

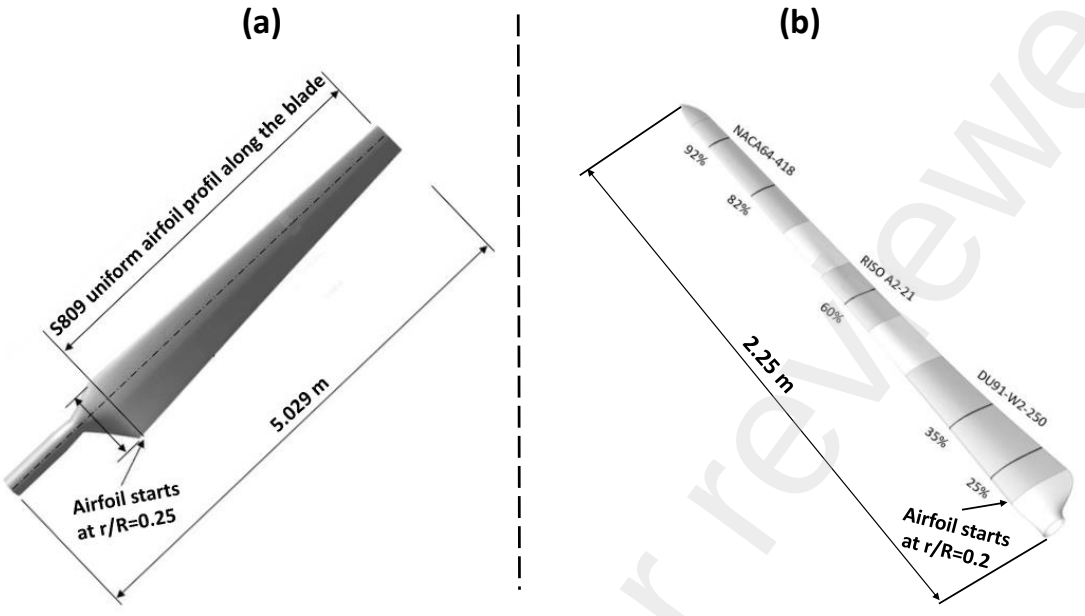

Figure 6: Overview of (a) the NREL Phase VI rotor and (b) the MEXICO wind turbine blade.

6. Case study: application of the new algorithm to the NREL Phase VI and the MEXICO wind turbines

To evaluate the effectiveness of the newly developed algorithm, simulations were conducted for the aerodynamic design and optimization of the NREL Phase VI and MEXICO HAWT, described as follows:

The NREL (National Renewable Energy Laboratory) Phase VI wind turbine is equipped with a two-bladed, 10.058 m diameter upwind rotor that operates at a constant rotational speed of 72 rpm in a counter-clockwise direction. The blade's chord and twist change progressively from the root to the tip. The blades of the NREL Phase VI turbine have a general pitch angle of $\theta_0 = 3°$ and a coning angle of $\gamma = 0°$, consisting of a uniform S809 aerodynamic profile from the aerodynamically profiled station at $\frac{r}{R} = 0.25$ to the tip, as illustrated in Fig. 6.(a). Although not extensively documented in literature, it is noted that the NREL Phase VI HAWT is expected to generate a nominal power of 19.8 kW at a wind speed of 12 m/s. However, results from the NREL/NASA AMES Wind Tunnel Experiments indicated that the turbine's mechanical power output does not surpass 10 kW due to sub-optimal blade characteristics.

On the other hand, the MEXICO (Model EXperiments In Controlled cOnditions) wind turbine comprises a three-bladed, 4.5 m diameter upwind rotor that rotates at 425 rpm in the clockwise direction. The blade's chord and twist also vary radially from root to tip. The MEXICO rotor blade features a global pitch angle of $\theta_0 = -2.3°$ and a coning angle of $\gamma = 0°$. The blade utilizes three distinct aerodynamic profiles, depicted in Fig. 6.(b): DU91-W2-250 from 20% to 45.5% of the radial position, RISØ-A1-21 from 54.4% to 65.5%, and NACA 64-418 from 74.4% to the blade tip. The MEXICO blade is optimized for peak performance at a wind speed of 15 m/s, corresponding to a tip-speed ratio (TSR) of 6.67.

In this section, the primary design geometries derived from the proposed design algorithm would be introduced. This algorithm generates non-linear local chord and twist distributions for both the NREL Phase VI and MEXICO wind turbines. Additionally, these distributions would be linearized at various radial stations starting from different floating roots. The aim is to identify the most effective radial station for blade linearization. Following the optimization of blade characteristics, comparison of the best linearized pattern would be carried out with the design models obtained using the actual rotor models, as described in Sec. 6. This approach aligns with the methodology employed by Alkhabbaz et al. [39] in designing a 10 kW small HAWT. Subsequently, the optimal design approach would be assessed by examining the distribution of the power coefficient against the free-stream velocity, along with the annual energy production (AEP). This evaluation particularly considers the flow conditions prevalent in the In Salah region [58]. The

performance of the optimized design is compared against that of the baseline model. Lastly, given that the MEXICO wind turbine is the only HAWT model with comprehensive full-scale PIV measurements, the influence of aerodynamic optimizations on the expansion of the near wake would be explored at the design wind speed U_{Design}.

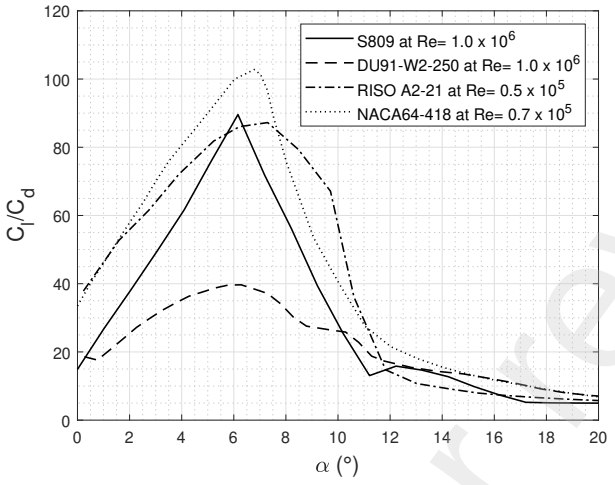

Figure 7: The glide ratio variation ($\frac{C_l}{C_d}$) versus the angle of attack α for the S809, DU91-W2-250, RISØ-A1-21 and NACA64-418 respectively [47, 48, 49, 50].

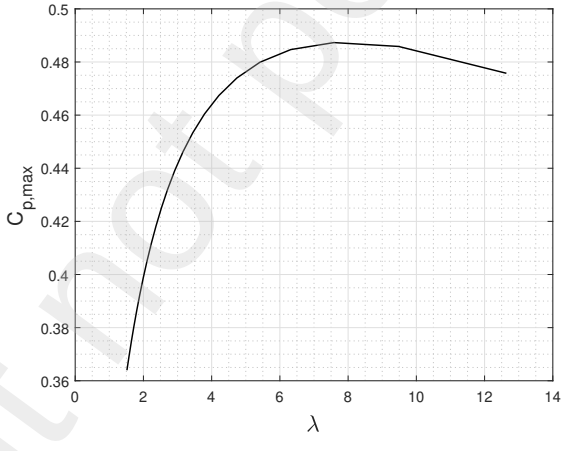

Figure 8: The estimated maximum power coefficient versus the tip speed ratio λ.

6.1. HAWT aerodynamic design

Fig. 7 illustrates the variation of the glide ratio $\left(\frac{C_l}{C_d}\right)$ with respect to the angle of attack (α) across four aerodynamic profiles used in both the NREL Phase VI and MEXICO wind turbine blades. For the S809 profile on the NREL Phase VI rotor blade specifically designed for HAWT applications by the NREL, the glide ratio achieves a peak of 89.60 at an angle of attack $\alpha_{op} = 6.16°$. This angle represents the optimal design point selected during the blade design phase. Conversely, for the MEXICO rotor blade airfoils, the highest glide ratios for the DU91-W2-250, RISØ-A1-21, and NACA 64-418 profiles occur at angles of attack of 6.28°, 7.20°, and 6.80°, respectively. Technically, these turbines generate approximately 80% of their energy in the upper mid-span region of the blade, where the near-root section facilitates turbine start-up [59]. In this study, an optimal angle $\alpha_s = 7°$ was selected for the design of the HAWT operating at a design wind speed $U_{Design} = 15$ m/s.

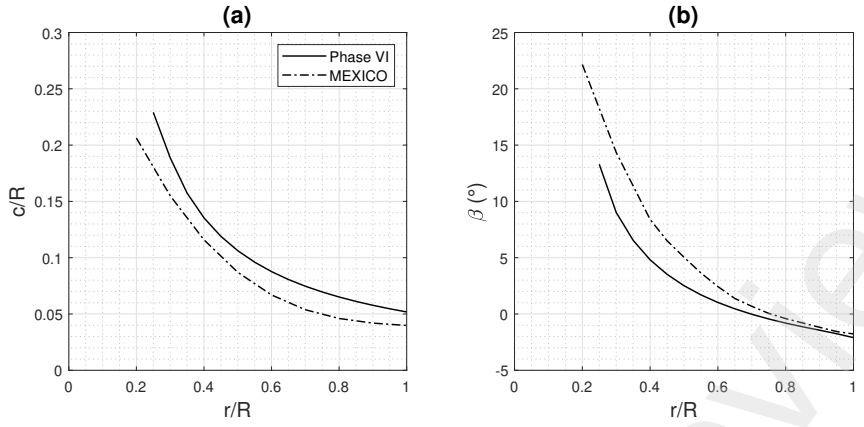

Figure 9: Radial distribution of the primary (1) chord (c/R) and (2) twist (β) over (a) the NREL Phase VI and (b) MEXICO rotor blades.

Contrary to the MEXICO wind turbine, the NREL Phase VI HAWT does not have a specified design wind speed, U_{Design}, provided by its manufacturer. Consequently, extensive research has been conducted to ascertain the design wind speed that maximizes the aerodynamic performance based on Wilson et al.'s methodology [60], as shown in Eq. (24). This formula calculates the highest achievable power coefficient for wind turbines with an optimal blade configuration and a finite number of blades. Fig. 8 illustrates the variation of the maximum achievable power coefficient against λ, indicating that the ideal tip speed ratio ($\lambda = 7.583$) corresponds to an average incoming free stream velocity of $U_0 = U_{\text{averaged}} = 5.00$ m/s, yielding an optimal power coefficient, C_p, of 0.487. Therefore, a design wind speed of $U_{\text{Design}} \approx 7.00$ m/s, calculated as $1.4 \times U_{\text{averaged}}$, has been selected in alignment with the IEC 61400-2 standard for small HAWT designs. This has led to the adoption of a new rotational speed, $\Omega = 100.8$ rpm, to preserve identical operational flow conditions.

$$C_{p,max} = (\frac{16}{27})\lambda[\lambda + \frac{1.32 + (\frac{\lambda-8}{20})^2}{B^{\frac{2}{3}}}]^{-1} - \frac{0.57\lambda^2}{\frac{C_l}{C_d}(\lambda + \frac{1}{2B})} \tag{24}$$

Figure 9 illustrates the primary (a) local chord and (b) twist distributions along the rotor blade for the NREL Phase VI and MEXICO wind turbines, respectively. For the NREL Phase VI turbine, the chord variation, as described by Eq. (21), diminishes non-linearly from the root towards the blade tip. At the initial profiled radial station, $\frac{r}{R} = 0.25$, the maximum chord and twist are recorded at $c/R = 0.23$ and $\beta = 13.29°$. Conversely, at the blade tip, the values decrease to $c/R = 0.0518$ and $\beta = -2.09°$. In contrast, the primary design algorithm applied to the MEXICO wind turbine reveals maximum local chord and twist values of $c/R = 0.2$ and $\beta = 22.15°$ at the first profiled station $\frac{r}{R} = 0.20$. At the tip, these values change to $c/R = 0.38$ and $\beta = -1.77°$. Despite achieving substantial power coefficients of $C_p = 0.4365$ for the NREL Phase VI and $C_p = 0.476$ for the MEXICO wind turbines, the complexity and high cost of manufacturing pose significant challenges. Therefore, linearization of the blade chord and twist, aimed at simplifying the manufacturing process, has been implemented as per Eq. (22).

The linearization of the blade chord and twist was implemented according to Eq. (22), anchoring the analysis at the primary blade tip while designating the radial positions $\xi = (\text{First profiled station}, 0.3, 0.4, \ldots, 0.8)$ along the blade span as the reference roots. This methodology was employed to pinpoint the initial profiled span-wise position that maximizes rotor performance. The resulting distributions of chord and twist, which are linear locally, are depicted in Fig. 10. It is important to note from a production perspective, a HAWT blade characterized by a linear distribution of chord and twist is generally simpler and more cost-effective to manufacture. A comparative analysis of the performance of these linearized geometries, particularly in terms of mechanical torque generated, was conducted to identify the optimal radial station for superior aerodynamic characteristics.

Fig. 11 illustrates the predicted aerodynamic mechanical torque across various linearization roots for the (a) NREL Phase VI and (b) MEXICO wind turbines. In the case of the NREL Phase VI (Fig. 11.(a)), the aerodynamic torque

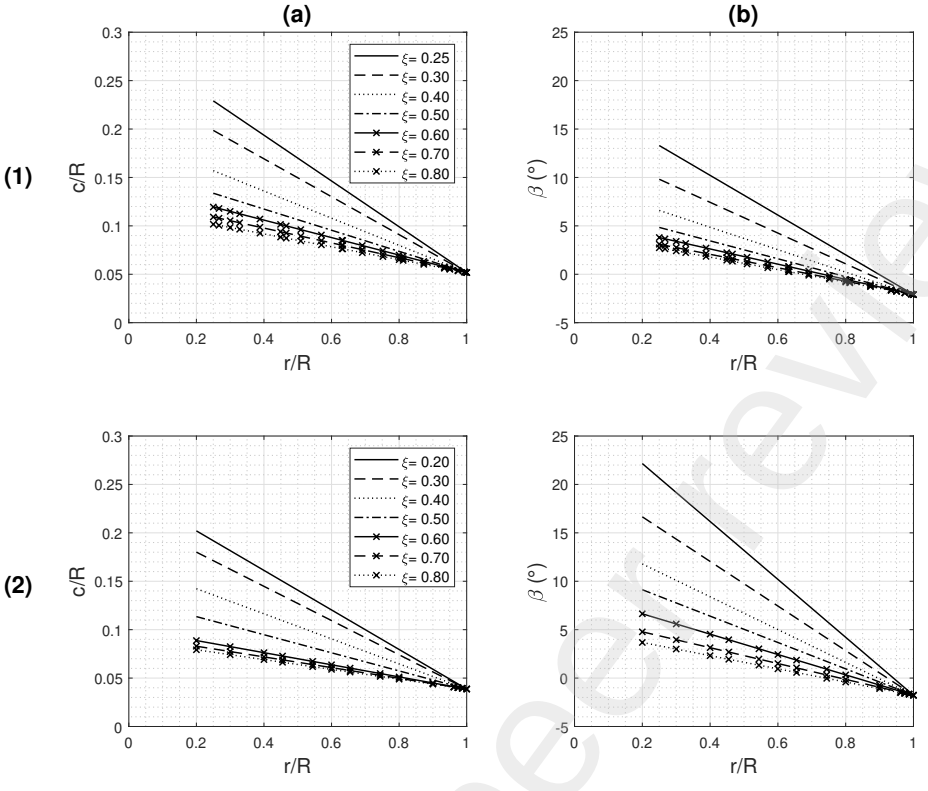

Figure 10: Radial distribution of the linearized (a) chord (c/R) and (b) twist (β) over the (1) NREL Phase VI and (2) MEXICO rotor blades.

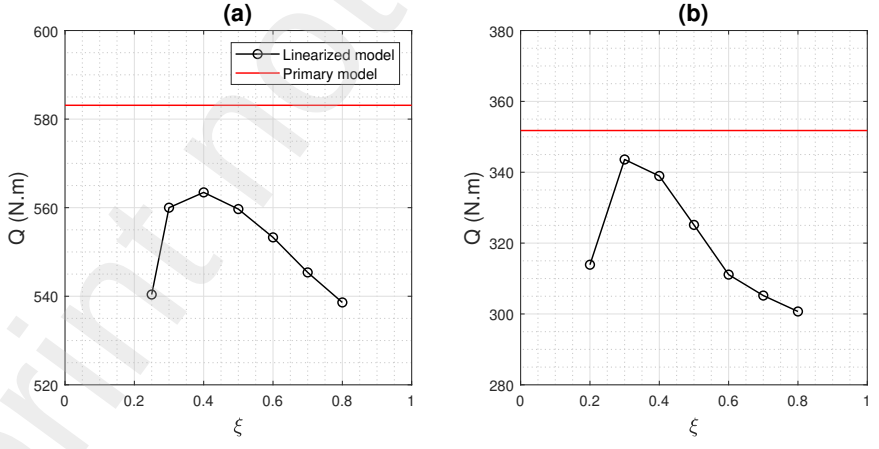

Figure 11: The predicted aerodynamic mechanical torque, obtained at different linearization roots ξ, for the (a) NREL Phase VI and (b) MEXICO wind turbines.

produced shows an increase with the rotor blade's radial position, reaching a peak of 564 N.m at the linearization root of $\xi = 0.4$. Beyond this point, an increase in the linearization root reduces the torque, with the minimum observed at $\xi = 0.8$. Conversely, the MEXICO wind turbine (Fig. 11.(b)) demonstrates its highest mechanical torque of 343.6 N.m at a linearization root of $\xi = 0.3$, which is distinct from the NREL case. This torque value diminishes as the linearization

root extends along the blade, bottoming out at $\xi = 0.8$. From these observations, the optimal radial position for root linearization concerning chord and twist adjustments on the rotor blade is determined to be within $\xi = [0.3\text{-}0.4]$.

6.2. HAWT aerodynamic performances study

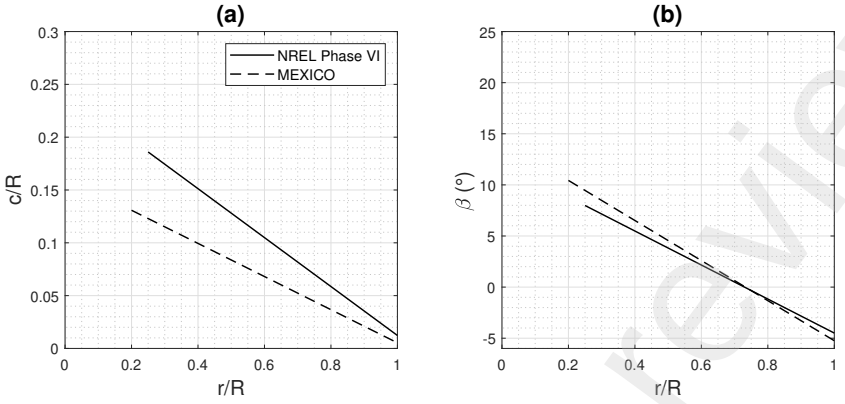

Figure 12: Resulting (a) chord and (b) twist distributions for the NREL Phase VI and MEXICO rotor obtained using the actual rotor model.

The initial task in this section is to determine the most efficient design method by employing blade linearization. It aims to evaluate the optimal linearized configurations against design outcomes derived from authentic rotor models, as outlined in Sec. 6. This strategy mirrors the process utilized by Alkhabbaz et al. [39] for the development of a 10 kW small-scale HAWT. By implementing the genuine rotor model detailed in Sec. B, the design and optimization of the NREL Phase VI and MEXICO wind turbines have been accomplished, resulting in specific chord and twist distributions. These are illustrated in Fig. 12 and are characterized as follows:

- The NREL Phase VI rotor: at the first profiled radial station ($r/R = 0.25$), a maximum value of the local chord and twist of $c/R = 0.186$ and $\beta = 6.00°$ have been obtained where at the blade tip radial station ($r/R = 1.00$), a local chord and twist values of $c/R = 0.0122$ and $\beta = -4.5°$ respectively have been recorded.

- The MEXICO rotor: a maximum value of the local chord and twist of $c/R = 0.13$ and $\beta = 10.43°$ have been recorded, at the first profiled span wise position ($r/R = 0.20$), where local chord and twist values of $c/R = 0.005$ and $\beta = -5.20°$ respectively have been recorded at the blade tip radial station ($r/R = 1.00$).

To substantiate the results achieved, an analysis of the radial distribution of elementary torque along the rotor blades of the (a) NREL Phase VI and (b) MEXICO wind turbines has been conducted, as illustrated in Fig. 13. This analysis aims to evaluate the aerodynamic performance of both the original rotor models and a newly introduced design methodology, with the objective of identifying superior blade features for Horizontal Axis Wind Turbines (HAWT). The evaluation was performed at design wind speeds, with free stream velocities of (a) $U_{Design} = 7.0$ m/s and (b) $U_{Design} = 15$ m/s. For the NREL Phase VI rotor, depicted in Fig. 13.(a), the optimized model derived from the innovative design approach matches the aerodynamic performance of the original rotor model from the blade root to the mid-span. Beyond this region, the hybrid model demonstrates a marked enhancement in performance in the upper mid-span sections, unlike the original model which exhibits a decline. In the case of the MEXICO wind turbine, as shown in Fig. 13.(b), the original rotor design underperforms across the entire blade length, from root to tip, in comparison to the hybrid model. Notably, significant improvements are observed at the upper mid-span, where the primary mechanical torque of the wind turbine is generated. These outcomes validate that the aerodynamic characteristics predicted by the new HAWT model design are superior throughout the rotor blade, thus confirming the efficacy of the newly proposed design algorithm.

Fig. 14 illustrate the performance of three different wind turbine models: Primary, Optimized, and Baseline respectively, by plotting the predicted power coefficient C_p against the free stream velocity U_0 for two specific turbines: the NREL Phase VI (Fig. 14.(a)) and the MEXICO wind turbines (Fig. 14.(b)). This investigation aims to display the

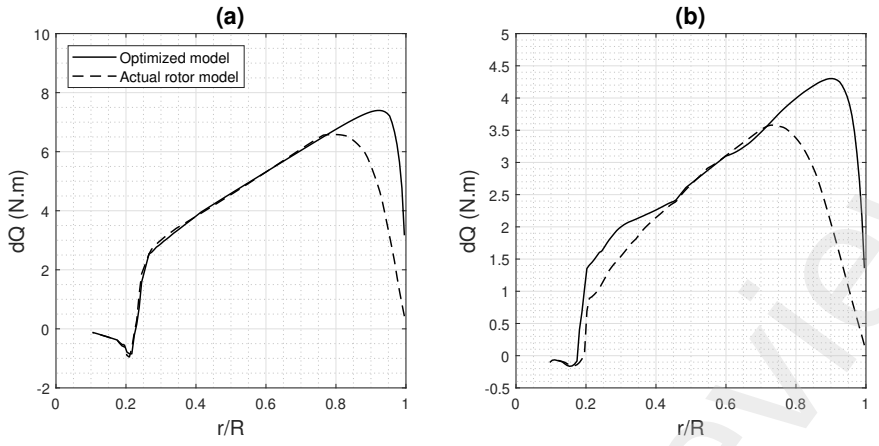

Figure 13: Radial distribution of the predicted aerodynamic mechanical torque over the rotor blade of the (a) NREL Phase VI and (b) MEXICO wind turbines.

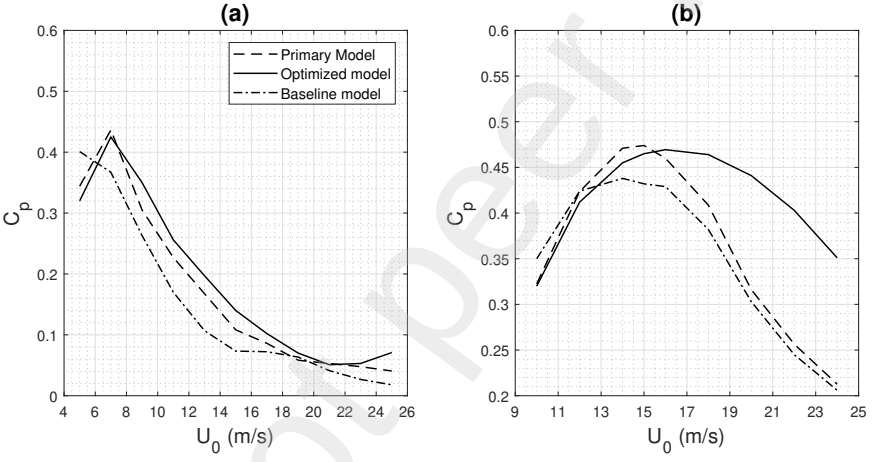

Figure 14: Variation of the predicted power coefficient C_p, versus the incoming free stream velocity U_0, obtained for the optimized and baseline designs of (a) the NREL Phase VI and (b) MEXICO wind turbines.

consistency of the presented subroutine as well as allows to compare between the existing, primary and the optimized HAWT models.

In Fig. 14.(a), the power coefficient C_p of both primary and optimized models increases with the free stream velocity U_0 until reaching a peak, beyond which it significantly decreases. This peak corresponds to the optimal velocity range U_{Design} for maximal power generation. Both the primary and optimized models exhibit a higher peak, achieving a maximal power coefficient of $C_p \approx 0.425$ ($P \approx 6.02$ kW), which surpasses the baseline model's $C_p = 0.375$ ($P = 5.24$ kW) by 13.33%, indicating an enhanced efficiency in converting wind energy at this peak. Upon increasing the incoming free stream velocity to $U_0 = 12$ m/s (TSR = 3.16), where the baseline model was expected to produce a rated power of 19.80 kW, its power coefficient predictions $C_p = 0.123$ ($P = 10.50$ kW) fall significantly short of the design specifications, with a substantial discrepancy of 116.73% (11.84 kW). The newly optimized design delivers superior performance with a power coefficient of $C_p = 0.2265$ ($P \approx 19.00$ kW), outperforming the primary model's $C_p = 0.1973$ ($P \approx 16.60$ kW). This represents a significant improvement of 50% over the baseline model from the NREL Phase VI. Initially, the primary and baseline models perform comparably to the optimized model but begin to exhibit a slight decline in power coefficient as the velocity increases.

For the MEXICO wind turbine, Fig. 14.(b) displays a narrower range of velocities and shows the C_p peaking around U_{Design}=15 m/s for all models. The Optimized and primary model again outperform the baseline model with a power

coefficient of C_p= 0.465 (P= 15.20 kW) and C_p= 0.473 (P= 15.93 kW) respectively, greater than the baseline model which has provided a power coefficient of C_p= 0.432 (P= 14.20 kW). By increasing the free stream velocity to an incoming free stream velocity of U_0= 24 m/s (TSR= 4.17), corresponding to a fully detached flow regime, it can be seen that the baseline and primary models power coefficient predictions are highly under-predicted compared to the optimized model with maximum shift of 70 %. This high recorded discrepancy corresponds to an important mechanical power augmentation of 19.37 kW.

Maintaining a higher C_p over a broader range of velocities, suggests that the turbine's optimized model, for both the NREL Phase VI and MEXICO HAWT, allow it to operate more efficiently across a wider range of conditions. The curves for the Primary and Baseline models are very similar, indicating minimal differences in their design or operational efficiencies under these specific conditions.

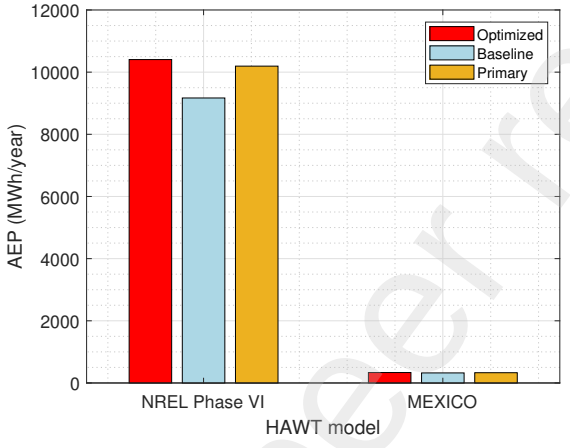

Figure 15: Estimated annual energy production calculated for the Optimized (red), Baseline (blue) and Primary (Yellow) designs of the NREL Phase VI and MEXICO wind turbines.

The assessment of the optimal blade design includes the consideration of Annual Energy Production (AEP). AEP is characterized as the average effective power generated by the wind turbine throughout a year, and its estimation involves the application of the equation defined in Sec. C. The AEP has been calculated based on the flow features of In Salah [58] located in the south of Algeria, it is characterized by an annual mean wind speed ($AMWS$) of 6.4 m/s, depicted at an altitude of 10 m, with Weibull shape and scale parameters of $k^{'} = 2.39$ and $c^{'} = 7.2$ m/s respectively. This $AMWS$ corresponds mostly to the NREL Phase VI design wind speed U_{Design}= 7 m/s, in contrary to the MEXICO wind turbine case U_{Design}= 15 m/s; thus, the effect of the aerodynamic design would be effective and noticeable for the NREL Phase VI optimization study.

Fig. 15 illustrates the estimated annual energy production (AEP), measured in MWh/year, for two models of Horizontal Axis Wind Turbines (HAWT): NREL Phase VI and MEXICO. The AEP is presented for Optimized (red), Baseline (blue) and Primary (Yellow) designs of these models. The NREL Phase VI project showcases distinct differences in annual energy production (AEP) across three designs. The optimized design, depicted by the red bar, stands out with an AEP of approximately 10,404 MWh/year, reflecting the success of the proposed aerodynamic optimization strategy. The baseline design, represented by the blue bar, achieves an AEP of around 9,168 MWh/year, serving as the fundamental reference model with standard features. Meanwhile, the primary design, marked by the yellow bar, offers a slight improvement over the baseline, with an AEP close to 10,193 MWh/year, incorporating minor enhancements to boost efficiency. In the case of the MEXICO wind turbine, designed for a high wind speed of U_{Design} = 15 m/s, which is significantly higher than the $AMWS$ at the In Salah site, the influence of aerodynamic optimization on the Annual Energy Production (AEP) is relatively modest, with an observed increase of only 3.7%. The rotor of the MEXICO wind turbine, being a contemporary design, is optimized to deliver peak performance at elevated free stream velocities, as illustrated in Fig. 14(b).

It should be noted that the process of blade linearization not only simplifies the manufacturing approach but also impacts the predicted aerodynamic characteristics. The Study has shown that initial models featuring non-linear blade chord and twist yield performances nearly equivalent to those of the design conditions. Nevertheless, at higher incom-

ing wind speeds, a decrease in performance is observed.

6.3. HAWT near wake study

The influence of aerodynamic enhancements on the expansion of the near wake behind the rotor of a Horizontal-Axis Wind Turbine (HAWT) is a critical element in analyzing interactions among wind turbines, which further aids in the refinement of wind farm layouts. The MEXICO wind turbine, uniquely characterized by full-scale Particle Image Velocimetry (PIV) measurements, serves as the solitary contemporary HAWT model equipped for such studies. This research primarily focuses on the axial profiles of axial and radial velocity components, which are crucial for evaluating the velocity deficit and the expansion of the stream tube post-HAWT rotor. These assessments will be conducted at the design incoming free stream velocity of $U_{\text{Design}} = 15$ m/s, under which the MEXICO HAWT rotor achieves optimal flow conditions.

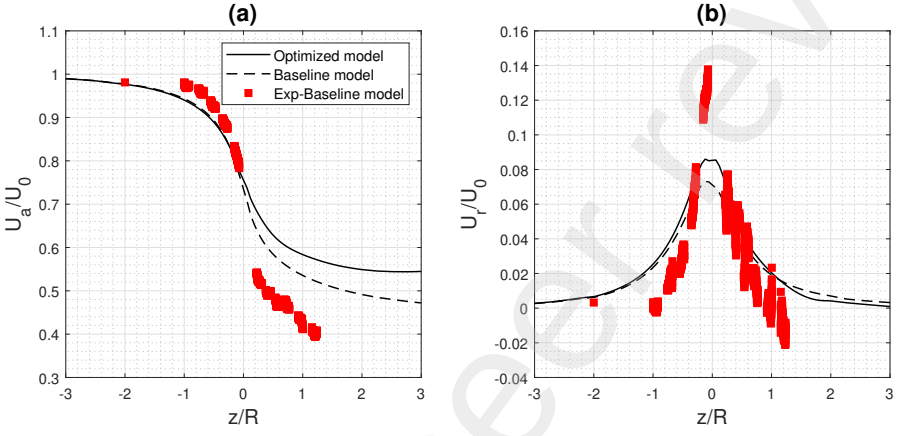

Figure 16: Axial distribution of the (a) axial and (b) radial velocity components, obtained for the Baseline and Optimized models at an incoming free stream velocity of U_0= 15 m/s, upstream and downstream from the rotor at an axial distance of z/R= $\pm$3 and radial station of r= 1.5 m.

Fig. 16 illustrates the axial profiles of (a) axial and (b) radial velocity components for both the Baseline and Optimized models under a free stream velocity of $U_0 = 15$ m/s, examined upstream and downstream of the rotor at an axial distance of $z/R = \pm 3$ and a radial position of $r = 1.5$ m. In Fig. 16(a), the Baseline model exhibits a notable reduction in axial velocity by approximately 15%, located downstream of the HAWT rotor, in contrast to the Optimized model. This reduction in velocity leads to a marked decrease in aerodynamic performance, especially when applied to a wind farm scenario downstream, potentially escalating the cost of energy production. Conversely, as shown in Fig. 16(b), the Optimized model demonstrates an increase in radial velocity at the rotor plane by about 16.75%. This enhancement can be attributed to the optimal axial induction achieved through the optimization process, which effectively enlarges the flow stream tube, thereby improving the aerodynamic performance.

7. Conclusions

This research develops a hybrid methodology for the aerodynamic design and performance optimization of Horizontal Axis Wind Turbine (HAWT) blades, offering a significant advancement over the traditional Blade Element Momentum (BEM) method. This innovative approach integrates critical aerodynamic factors such as turbulence, viscosity, non-uniform pressure distribution, and multidimensional flow fields into the design process. Renowned for its computational efficiency, this method avoids the extensive resource requirements of full Navier-Stokes simulations. Utilizing the Actuator Disk Method (ADM), the study leverages Reynolds Averaged Navier-Stokes equations and the $k-\omega$ Shear Stress Transport (SST) turbulence model [53] to refine blade design. Specifically, it introduces an effective strategy for the local distribution and linearization of chord and twist configurations, seamlessly integrated into a custom axisymmetric actuator disk subroutine in OpenFOAM. This optimized numerical model significantly enhances the aerodynamic performance of small HAWTs, specifically the NREL Phase VI and MEXICO models, according to comprehensive computational analyses. The following findings have been highlighted through this study:

- A revised rotational speed of Ω= 100.8 rpm is suggested for the NREL Phase VI wind turbine, which aligns with the enhanced performance characteristics observed in simulation. This adjustment optimizes the turbine's operation under typical wind conditions, potentially increasing its energy capture and efficiency. Further investigation into variable speed operations could provide additional benefits in adapting to fluctuations in wind speed, thereby maximizing energy yield.

- The optimal radial location for initiating chord and twist linearization is identified between ξ= 0.3 and 0.4. This finding emphasizes the importance of precise geometric modifications at specific sections of the blade to leverage aerodynamic benefits effectively. Extending this analysis to include the effects of these modifications on blade stress distribution and fatigue life could provide deeper insights into their practical implementation.

- Compared to the existing models, the hybrid design significantly enhances power and torque outputs, particularly in the upper mid-span of the blades. This improvement suggests that the hybrid model is particularly effective in capturing and converting wind energy in this critical section of the blade. Future designs could explore the application of similar methodologies to different blade sections or even entire rotor systems to assess their potential for overall performance improvement.

- The aerodynamic performance of the redesigned blades surpasses that of the original models in terms of both power coefficient and annual energy production. This superior performance not only validates the hybrid design approach but also suggests its potential applicability to other turbine models and designs. Further comparative studies involving different turbine configurations under various operational conditions would help in generalizing these findings.

- The aerodynamic interference behind the rotor, as measured by velocity deficit, is reduced in the redesigned model, suggesting potential improvements in wind farm efficiency. This reduction could potentially facilitate closer spacing of turbines within wind farms, thereby maximizing land use and overall farm output. Additional studies on the interaction between multiple turbines in a farm setting could help in optimizing farm layouts to exploit this reduced interference effectively.

Future work could further investigate these enhancements in turbine performance by incorporating more diverse environmental conditions and operational scenarios. Including a broader range of turbine sizes and configurations would also test the robustness and scalability of the proposed hybrid design methodology. Additionally, the integration of these aerodynamic improvements with structural and economic models could provide a holistic view of the turbine design and operation, leading to better-informed decisions in wind turbine production and deployment.

Acknowledgments

The authors thank the Directorate-General for Scientific Research and Technological Development (DGSRDT) of Algerian government.

Appendix

A. Mesh sensitivity study

A study on mesh sensitivity was conducted using the characteristics of the MEXICO wind turbine, described in Sec. 6, with an inflow velocity of $U_0 = 15$ m/s. This study aimed to identify the optimal mesh granularity for Actuator Disk Method (ADM) simulations near the Horizontal Axis Wind Turbine (HAWT) rotor. Accurate simulation of the flow in the rotor's near wake is critical, necessitating a detailed examination of mesh effects both upstream and downstream of the rotor center. The findings, illustrated in Fig. 17, indicate minimal variations in axial and radial velocity components at a distance of $\frac{z}{R} = 0.13R$ from the rotor in both directions, achieved with a mesh resolution of D/64. Nevertheless, as shown in Fig. 18, significant velocity fluctuations at the rotor plane suggest the need for finer mesh resolution to enhance the accuracy of predictions. It was found that increasing the mesh refinement to D/128 sufficiently resolves the flow dynamics around the HAWT rotor.

The study on the influence of the number of actuator points (N_b) incorporates a parameter Λ, detailed in Eq. (25). This parameter quantifies the difference between the output power obtained with a large count of actuator elements

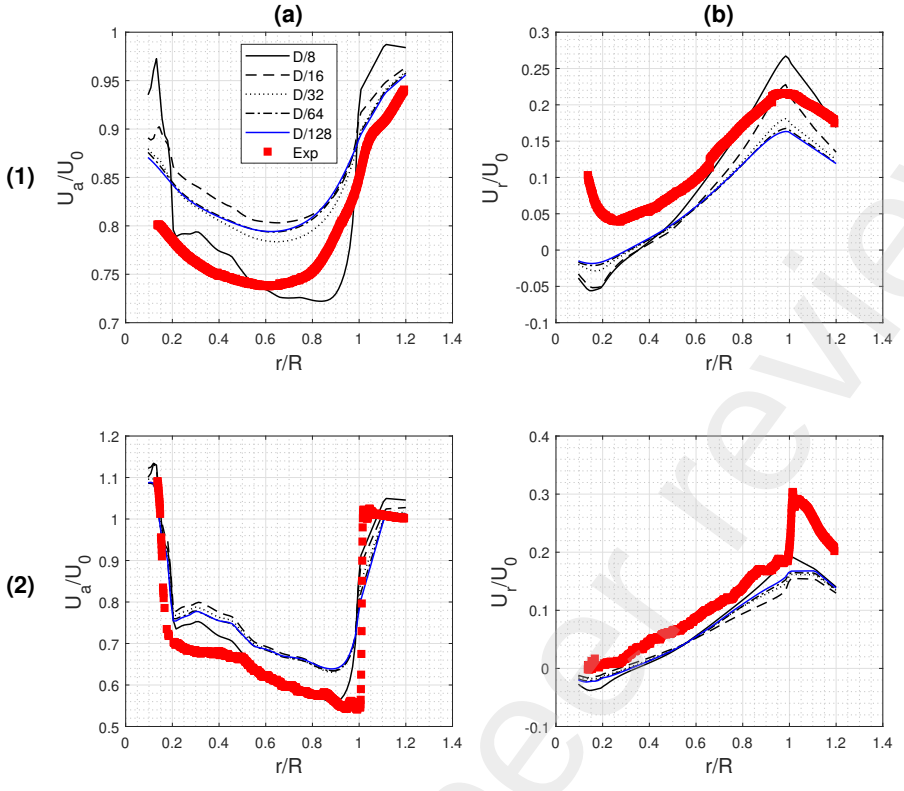

Figure 17: Radial distribution of the (a) axial and (b) radial velocity components, obtained at an incoming free stream velocity of U_0= 15 m/s, (1) upstream and (2) downstream from the rotor at an axial distance of z/R= $^+_-$0.13.

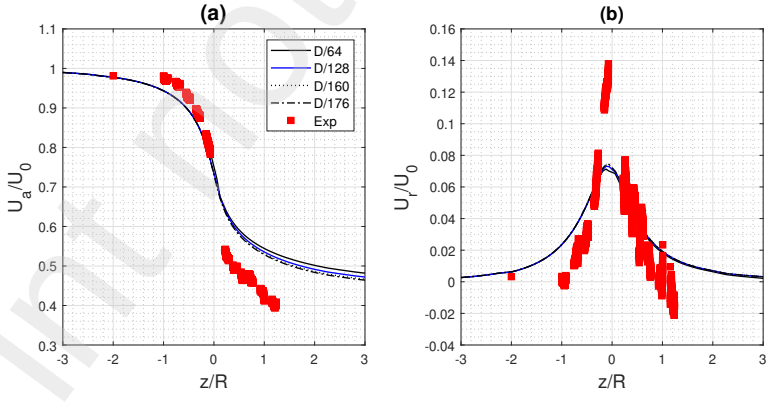

Figure 18: Axial distribution of the (a) axial and (b) radial velocity components, obtained at an incoming free stream velocity of U_0= 15 m/s, upstream and downstream from the rotor at an axial distance of z/R= $^+_-$3 and radial station of r= 1.5 m.

(designated here as $N_\infty = N_{256}$) and various incremental actuator element counts. As demonstrated in Fig. 19, the stability of the torque output is evident once the number of actuator points (N_b) reaches 128. Beyond this point, further increases in N_b do not significantly alter the torque predictions. Thus, an optimal number of actuator elements has been established at $N_b = 128$.

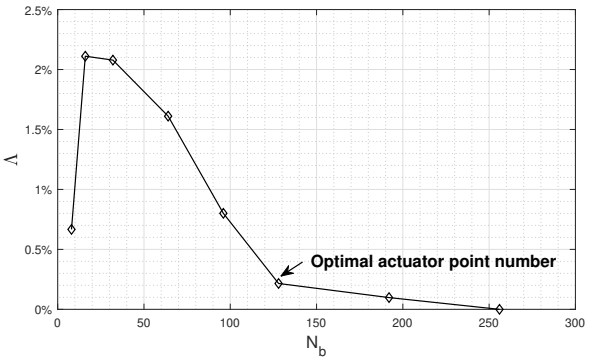

Figure 19: Actuator elements number (N_b) dependency study.

$$\Lambda = \frac{P(N_\infty) - P(N_b)}{P(N_\infty)} \tag{25}$$

B. Actual rotor model

Several theoretical frameworks exist to forecast aerodynamic behavior and to ascertain the most suitable chord length and distribution of twist angles for optimal performance [32, 54]. Typically, Betz's theory is adopted for the design of HAWT blades, though it overlooks the effects of turbulence and rotational forces at the blade tips. The Blade Element Momentum (BEM) theory is commonly applied to determine the ideal rotor configuration, which includes computing the optimal chord and twist for each segment of the blade, described by the equation below:

$$\begin{cases} \phi_i = \frac{2}{3} tan^{-1}(\frac{1}{\lambda_{r,i}}) \\ c_i = \frac{8\pi r_i}{BC_{l,op,i}}(1 - cos(\phi_i)) \\ \beta_i = \phi_i - \alpha_{op} \end{cases} \tag{26}$$

The enhanced Blade Element Momentum (BEM) model, which accounts for the effects of the tip loss factor and wake expansion, is often termed the actual rotor model. This model employs an iterative method to ascertain the optimal axial and tangential induction factors. The detailed process for iterative rotor design is summarized as follows:

1. the initial values for both the axial and tangential induction factor have been determined based on the design values from the ideal rotor configuration and calculated as follows:

$$\begin{cases} a_{i,1} = \frac{1}{[1+\frac{4sin^2(\phi_{i,1})}{\sigma_{op,i}C_{l,op}cos(\phi_{i,1})}]} \\ a'_{i,1} = \frac{1-3a_{i,1}}{4a_{i,1}-1} \\ \sigma_i = \frac{Bc_i}{2\pi r_i} \end{cases} \tag{27}$$

   where i denotes the ith blade station, $\sigma_{op,i}$ signifies the local solidity derived from the primary blade design. The parameters $a_{i,1}$ and $a'_{i,1}$ refer to the axial and tangential induction factors for the specified section.

2. With initial estimates for $a_{i,1}$ and $a'_{i,1}$ in place, initiate the iterative solution process for the jth iteration. Begin with j= 1 for the first iteration. Compute the angle relative to the wind using the following equation, then, compute the tip loss factor using Eq. (4):

$$\phi_{i,j} = tan^{-1}(\frac{1 - a_{i,j}}{(1 + a'_{i,j})\lambda_{r,i}}) \tag{28}$$

3. Calculate the yielding angle of attack $\alpha_{i,j}$ and determine the corresponding airfoil lift and drag coefficients ($C_{l,i,j}$, $C_{d,i,j}$) respectively.

$$\alpha_{i,j} = \phi_{i,j} - \beta_{i,j} \tag{29}$$

where in the initial iteration with j= 1, the twist angle values are derived from the primary blade design.

4. Calculate the local thrust coefficient :

$$C_{T_r,i,j} = \frac{\sigma_i(1-a_{i,j})^2(C_{l,i,j}cos(\phi_{i,j}) + C_{d,i,j}sin(\phi_{i,j}))}{sin^2(\phi_{i,j})} \tag{30}$$

5. update the axial and tangential induction factors (a, $a^{'}$):

$$\begin{cases} a_{i,j} = \frac{1}{[1+\frac{4F_{i,j}sin^2(\phi_{i,j})}{\sigma_i C_{l,j}cos(\phi_{i,j})}]} & \text{if} \quad C_{T_r,i,j} < 0.96 \\ a_{i,j} = (1/F_{i,j})[0.143 + \sqrt{0.0203 - 0.6427(0.889 - C_{T_r,i,j})}] & \text{if} \quad C_{T_r,i,j} > 0.96 \\ a^{'}_{i,j} = \frac{1}{\frac{4F_{i,j}cos(\phi_{i,j})}{\sigma_i C_{l,j}} - 1} \end{cases} \tag{31}$$

6. The process (2-5) is reiterated until the latest induction factors $j+1$ converge within an acceptable tolerance level relative to the preceding values j.
7. The yielding primary chord and twist radial distributions would be linearized based on the findings of Alkhabbaz et al. [39] where the best linearization technique consists of considering the blade tip and the radial station of $\frac{r}{R}$= 0.3 as fixed roots to determine the value of the blade first profiled station.

C. Annual Energy Production

The annual energy production (AEP), representing the average effective power generated by the wind turbine throughout a year, has been estimated as follows [32]:

$$\begin{cases} AEP = 8760\ P_{wind}\ [\int_{cut\ in}^{cut\ out} C_p(U) f(U)\, dU\ ] \\ f(U) = (\frac{k^{'}}{c^{'}})(\frac{U}{c^{'}})^{k^{'}-1} exp(-(\frac{U}{c^{'}})^{k^{'}}) \end{cases} \tag{32}$$

where $f(U)$, $k^{'}$ and $c^{'}$ are the wind speed distribution based on Weibull probability, the Weibull shape parameter and the Weibull scale parameter respectively. The Weibull shape and scale parameters are calculated as follows [61]:

$$\begin{cases} k^{'} = N[\frac{\sum_{i=1}^{N} U_i^{k^{'}} ln(U_i)}{\sum_{i=1}^{N} U_i^{k^{'}}} - \sum_{i=1}^{N} ln(U_i)]^{-1} \\ c^{'} = [\frac{1}{N}\sum_{i=1}^{N} U_i^{k^{'}}]^{1/k^{'}} \end{cases} \tag{33}$$

where it should be noted that the Weibull shape parameter $k^{'}$ is calculated iteratively than injected for the Weibull scale parameter $c^{'}$ calculation.

References

[1] Eva Topham and David McMillan. Sustainable decommissioning of an offshore wind farm. *Renewable Energy*, 102:470–480, 2017.

[2] V. Santhanagopalan, M.A. Rotea, and G.V. Iungo. Performance optimization of a wind turbine column for different incoming wind turbulence. *Renewable Energy*, 116:232–243, 2018.

[3] M. Jureczko, M. Pawlak, and A. Mężyk. Optimisation of wind turbine blades. *Journal of Materials Processing Technology*, 167(2):463–471, 2005.
[4] Yingjue Li, Kexiang Wei, Wenxian Yang, and Qiong Wang. Improving wind turbine blade based on multi-objective particle swarm optimization. *Renewable Energy*, 161:525–542, 2020.
[5] Khaled Yassin, Aya Diab, and Zakaria Ghoneim. Aerodynamic optimization of a wind turbine blade designed for egypt's saharan environment using a genetic algorithm. *Renewable Energy and Sustainable Development*, 1(1):106–112, 2015.
[6] Amir Nejat and Hamid Reza and Kaviani. Aerodynamic optimization of a megawatt class horizontal axis wind turbine blade with particle swarm optimization algorithm. *Modares Mechanical Engineering*, 16(11), 2017.
[7] Hamid Moradtabrizi, Edris Bagheri, Amir Nejat, and Hamid Kaviani. Aerodynamic optimization of a 5 megawatt wind turbine blade. *Energy Equipment and Systems*, 4(2):133–145, 2016.
[8] Abdelhamid Bouhelal, Ahmed Ladjal, and Arezki Smaili. Blade element momentum theory coupled with machine learning to predict wind turbine aerodynamic performances. In *AIAA SCITECH 2023 Forum*, page 1153, 2023.
[9] M. N. Hamlaoui, A. Smaili, and H. Fellouah. Improved bem method for hawt performance predictions. In *2018 International Conference on Wind Energy and Applications in Algeria (ICWEAA)*, pages 1–6. IEEE, 2018.
[10] Abdelhamid Bouhelal, Arezki Smaili, Ouahiba Guerri, and Christian Masson. Comparison of bem and full navier-stokes cfd methods for prediction of aerodynamics performance of hawt rotors. In *2017 International Renewable and Sustainable Energy Conference (IRSEC)*, pages 1–6. IEEE, 2017.
[11] Hakjin Lee and Duck-Joo Lee. Numerical investigation of the aerodynamics and wake structures of horizontal axis wind turbines by using nonlinear vortex lattice method. *Renewable Energy*, 132:1121–1133, 2019.
[12] Néstor Ramos-García, Mads Mølholm Hejlesen, Jens Nørkær Sørensen, and Jens Honoré Walther. Hybrid vortex simulations of wind turbines using a three-dimensional viscous–inviscid panel method. *Wind Energy*, 20(11):1871–1889, 2017.
[13] M.N. Hamlaoui, A. Smaili, I. Dobrev, M. Pereira, H. Fellouah, and S. Khelladi. Numerical and experimental investigations of hawt near wake predictions using particle image velocimetry and actuator disk method. *Energy*, 238:121660, 2022.
[14] Idriss Ammara, Christophe Leclerc, and Christian Masson. A viscous three-dimensional differential/actuator-disk method for the aerodynamic analysis of wind farms. *J. Sol. Energy Eng.*, 124(4):345–356, 2002.
[15] Christian Masson, Arezki Smaïli, and Christophe Leclerc. Aerodynamic analysis of hawts operating in unsteady conditions. *Wind Energy*, 4(1):1–22, 2001.
[16] Yixiao Shao, Jie Su, Yu Tu, Limin Kuang, Zhaolong Han, Kai Zhang, and Dai Zhou. Assessment of the aerodynamic benefits of collocating horizontal-and vertical-axis wind turbines in tandem using actuator line model. *Physics of Fluids*, 35(7), 2023.
[17] Jörn Nathan, Christian Masson, and Louis Dufresne. Near-wake analysis of actuator line method immersed in turbulent flow using large-eddy simulations. *Wind Energy Science*, 3(2):905–917, 2018.
[18] Christophe Sibuet Watters, Simon-Philippe Breton, and Christian Masson. Application of the actuator surface concept to wind turbine rotor aerodynamics. *Wind Energy*, 13(5):433–447, 2010.
[19] Christian Masson and Christophe Sibuet Watters. Moving actuator surfaces: a new concept for wind turbine aerodynamic analysis. In *Proceedings of the international conference on renewable energies and power quality*, 2008.
[20] A Bouhelal, A Smaili, O Guerri, and C Masson. Numerical investigations on the fluid behavior in the near wake of an experimental wind turbine model in the presence of the nacelle. *Journal of Applied Fluid Mechanics*, 16(1):21–33, 2022.
[21] A Bouhelal, A Smaili, O Guerri, and C Masson. Numerical investigation of turbulent flow around a recent horizontal axis wind turbine using low and high reynolds models. *Journal of Applied Fluid Mechanics*, 11(1):151–164, 2018.
[22] Abdelhamid Bouhelal, Ouahiba Guerri, Arezki Smaili, and Christian Masson. Contribution to the aerodynamic study of the air-sand flow around a wind turbine blade installed in desert environment of algeria. In *2018 International Conference on Wind Energy and Applications in Algeria (ICWEAA)*, pages 1–6. IEEE, 2018.
[23] Abdelhamid Bouhelal, Arezki Smaïli, Christian Masson, and Ouahiba Guerri. Effects of surface roughness on aerodynamic performance of horizontal axis wind turbines. In *The 25th Annual Conference of the Computational Fluid Dynamics Society of Canada, CFD2017-337, University of Windsor*, pages 18–21, 2017.
[24] Abdelhamid Bouhelal, Christian Masson, Arezki Smaili, and Ouahiba Guerri. Evaluation of various turbulence models accuracy for prediction of hawt aerodynamics performance using new mexico measurements. In *International Symposium on Wind and Tidal Power ISWTP2017, Montreal, Canada*, pages 28–31, 2017.
[25] Vincent Dehouck, Mohamed Lateb, Jonathan Sacheau, and Hachimi Fellouah. Application of the blade element momentum theory to design horizontal axis wind turbine blades. *Journal of Solar Energy Engineering*, 140(1), 2018.
[26] W Zhong, Wen Zhong Shen, T Wang, and Y Li. A tip loss correction model for wind turbine aerodynamic performance prediction. *Renewable Energy*, 147:223–238, 2020.
[27] William John Macquorn Rankine. On the mechanical principles of the action of propellers. *Transactions of the Institution of Naval Architects*, 6, 1865.
[28] Robert Edmund Froude. On the part played in propulsion by differences of fluid pressure. *Transactions of the Institution of Naval Architects*, 30:390, 1889.
[29] NE Joukowski. Travaux du bureau des calculs et essais aeronautiques de l'ecole superièure technique de moscou. 1918.
[30] A. Betz. Schraubenpropeller mit geringstem energieverlust. mit einem zusatz von l. prandtl. *Nachrichten von der Gesellschaft der Wissenschaften zu Göttingen, Mathematisch-Physikalische Klasse*, 1919:193–217, 1919.
[31] H Glauert. Aerodynamic theory: A general review of progress, volume iv, chapter division l, airplane propellers, 1963.
[32] Martin OL Hansen. *Aerodynamics of wind turbines*. Routledge, 2015.
[33] Kyoungboo Yang. Geometry design optimization of a wind turbine blade considering effects on aerodynamic performance by linearization. *Energies*, 13(9):2320, 2020.

[34] Stefano Mauro, Rosario Lanzafame, Michele Messina, and Sebastian Brusca. How to extrapolate 3d aerodynamic coefficients from hawt cfd simulations: an inverse bem approach. In *Journal of Physics: Conference Series*, volume 2385, page 012128. IOP Publishing, 2022.
[35] Guodan Dong, Jianhua Qin, Zhaobin Li, and Xiaolei Yang. An inverse method for wind turbine blade design with given distributions of load coefficients. *Wind*, 2(1):175–191, 2022.
[36] Behnam Moghadassian and Anupam Sharma. Inverse design of single-and multi-rotor horizontal axis wind turbine blades using computational fluid dynamics. *Journal of Solar Energy Engineering*, 140(2):021003, 2018.
[37] Kenneth Loenbaek, Christian Bak, Jens I Madsen, and Michael McWilliam. A method for preliminary rotor design–part 1: Radially independent actuator disk model. *Wind Energy Science Discussions*, 2020:1–21, 2020.
[38] Mojtaba Tahani, Ghazale Kavari, Mehran Masdari, and Mojtaba Mirhosseini. Aerodynamic design of horizontal axis wind turbine with innovative local linearization of chord and twist distributions. *Energy*, 131:78–91, 2017.
[39] Ali Alkhabbaz, Ho-Seong Yang, A.H Samitha Weerakoon, and Young-Ho Lee. A novel linearization approach of chord and twist angle distribution for 10 kw horizontal axis wind turbine. *Renewable Energy*, 178:1398–1420, 2021.
[40] Germanischer Lloyd and Germany Hamburg. Guideline for the certification of wind turbines. *July 1st*, 2010.
[41] A Wimshurst and RHJ Willden. Analysis of a tip correction factor for horizontal axis turbines. *Wind Energy*, 20(9):1515–1528, 2017.
[42] Tony Burton, Nick Jenkins, David Sharpe, and Ervin Bossanyi. *Wind energy handbook*. John Wiley & Sons, 2011.
[43] Herman Snel, R Houwink, and J Bosschers. Sectional prediction of lift coefficients on rotating wind turbine blades in stall. In *ECN-C –93-052, Energy Research Centre of the Netherlands, ECN*, 1994.
[44] Zhaohui Du and Michael Selig. A 3-d stall-delay model for horizontal axis wind turbine performance prediction. In *1998 ASME Wind Energy Symposium*, page 21, 1998.
[45] Wen Zhong Shen, Robert Mikkelsen, Jens Nørkær Sørensen, and Christian Bak. Tip loss corrections for wind turbine computations. *Wind Energy: An International Journal for Progress and Applications in Wind Power Conversion Technology*, 8(4):457–475, 2005.
[46] David C. Wilcox. Reassessment of the scale-determining equation for advanced turbulence models. *AIAA Journal*, 26(11):1299–1310, 1988.
[47] JG Schepers, K Boorsma, and X Munduate. Final results from mexnext-i: Analysis of detailed aerodynamic measurements on a 4.5 m diameter rotor placed in the large german dutch wind tunnel dnw. In *Journal of Physics: Conference Series*, volume 555, page 012089. IOP Publishing, 2014.
[48] K. Boorsma and J.G. Schepers. Rotor experiments in controlled conditions continued: New mexico. *Journal of Physics: Conference Series*, 753:022004, sep 2016.
[49] David Simms, Scott Schreck, Maureen Hand, and Lee Jay Fingersh. Nrel unsteady aerodynamics experiment in the nasa-ames wind tunnel: a comparison of predictions to measurements. Technical report, National Renewable Energy Lab., Golden, CO (US), 2001.
[50] Lee Fingersh, Dave Simms, Maureen Hand, Dave Jager, Jason Cotrell, Mike Robinson, Scott Schreck, and Scott M Larwood. Wind tunnel testing of nrel's unsteady aerodynamics experiment. In *20th ASME Wind Energy Symposium*, 2001.
[51] M. N. Hamlaoui, A. Bouhelal, A. Smaili, and H. Fellouah. An engineering approach to improve performance predictions for wind turbine applications: Comparison with full navier-stokes model and experimental measurements. *Journal of Applied Fluid Mechanics*, 17(7):1379–1397, 2024.
[52] P. K. Chaviaropoulos and M. O. L. Hansen. Investigating Three-Dimensional and Rotational Effects on Wind Turbine Blades by Means of a Quasi-3D Navier-Stokes Solver. *Journal of Fluids Engineering*, 122(2):330–336, 2000.
[53] Florian R Menter, Martin Kuntz, Robin Langtry, et al. Ten years of industrial experience with the sst turbulence model. *Turbulence, heat and mass transfer*, 4(1):625–632, 2003.
[54] James F Manwell, Jon G McGowan, and Anthony L Rogers. *Wind energy explained: theory, design and application*. John Wiley & Sons, 2010.
[55] Borja Plaza, Rafael Bardera, and Sergio Visiedo. Comparison of bem and cfd results for mexico rotor aerodynamics. *Journal of Wind Engineering and Industrial Aerodynamics*, 145:115–122, 2015.
[56] Mohammed Nadjib Hamlaoui, Arezki Smaili, and Hachimi Fellouah. New stall delay approach for hawt performance predictions using a cfd hybrid method. In *AIAA Scitech Forum*, 2021.
[57] Christopher J Greenshields et al. Openfoam user guide. *OpenFOAM Foundation Ltd, version*, 3(1):47, 2015.
[58] H Daaou Nedjari, S Kheder Haddouche, A Balehouane, and Ouahiba Guerri. Optimal windy sites in algeria: Potential and perspectives. *Energy*, 147:1240–1255, 2018.
[59] Peter J. Schubel and Richard J. Crossley. Wind turbine blade design. *Energies*, 5(9):3425–3449, 2012.
[60] Robert Elliott Wilson, P Lissaman, and Stel N Walker. Aerodynamic performance of wind turbines. Technical report, Oregon State Univ., Corvallis (USA), 1976.
[61] Kasra Mohammadi, Omid Alavi, Ali Mostafaeipour, Navid Goudarzi, and Mahdi Jalilvand. Assessing different parameters estimation methods of weibull distribution to compute wind power density. *Energy Conversion and Management*, 108:322–335, 2016.